

An Investigation of Solidification Conditions and Melt Treatment on Microporosity Formation

Keivan Davami^a, Mehrdad Shaygan^b

a-Islamic Azad University, Naeen Branch, Isfahan, Iran

keivandavami@yahoo.com

b-Islamic Azad University, Najafabad Branch, Isfahan, Iran

m.shaygan@yahoo.com

Mohammad Kazem Besharati Givi, Mahmud Mousavi Mashhadi

University of Tehran, Tehran, Iran

bgivi@ut.ac.ir, mmosavi@ut.ac

Abstract

Cast aluminum-silicon (Al-Si) alloys are used in automotive and industrial weight-sensitive applications because of the alloys' low density and excellent castability. The presence of trapped gas and/or shrinkage pores in certain locations within the casting has been shown to influence mechanical properties such as tensile strength and fatigue life. These micromechanical defects could be found anywhere in the casting depending on the processing conditions. A large amount of porosity located in the center of the casting may have no effect on the mechanical properties or fatigue performance. A smaller, isolated pore near a surface may have significant impact on mechanical properties. Hence, it is important to develop a comprehensive model to predict the size, location and distribution of microporosity in casting.

In this work, we model the effect of various casting process parameters on microporosity formation for equiaxed aluminum A356 alloy casting. The process parameters include the cooling rate, grain refiner, and eutectic modifier melt additions. The comparisons between the experimental results and the simulations demonstrate agreement and present various approaches that have been implemented successfully.

1. Introduction

The basic principles behind casting processes are straightforward. Molten metal of sufficiently low viscosity flows into cavities of complex shape and solidifies upon cooling. However, behind this simple principle lie many complicated reactions and phase transformations. If proper care is not taken, metal casting is prone to defects such as misruns, macroshrinkage (macroporosity), microporosity, segregation, hot tear, and residual stress. The design objective of contemporary foundry engineers is to choose an optimized geometry and process parameters that eliminate or minimize defect evolution while ensuring the desired microstructure.

1.1 Effects of Eutectic Modifiers and Grain Refiners on Microporosity Formation

1.1.1 Eutectic Modifiers

Aluminium alloys with silicon (Si) as the major alloying addition are used widely by the industry. However, the presence of the brittle, acicular silicon phase in the microstructure has shown negative effects on the mechanical properties of casting. It is because the brittle nature of the large silicon plates and the sharp edges of the coarse acicular silicon phase promote crack initiation and propagation. The eutectic can be refined by an alloying process known as modification. For aluminium-silicon alloys, this usually involves the addition of strontium (Sr) or sodium (Na) into the melt. Strontium modification is known to alter the amount, characteristics, and distribution of porosity in Al-Si castings. Although many theories have been proposed to account for these effects, most can be considered inadequate because of their failure to resolve contradictions and discrepancies in the literature. A major concern with the refinement of the Al-Si eutectic phase in Al-Si alloys by Sr modification is the increased tendency of microporosity formation [1]. In their study, C. M. Dinnis et al. found that no apparent differences in the amount, distribution, and morphology of porosity were observed between Sr-free and Sr-containing alloys with no or very small eutectic volume fractions. However, Sr modification significantly changed the amount, distribution, and morphology of porosity in alloys with a significant volume fraction of eutectic. The addition of Sr reduced porosity in the hot-spot region of casting, and the pores became well dispersed and rounded. This result can be explained by considering the combined effect of the casting design and the differences in the pattern of eutectic solidification between unmodified and Sr-modified alloys [2]. Figure 1 and Figure 2 show the microstructure of unmodified and modified A356 alloys, respectively.

J. Lacaze et al. found that strontium does not affect the primary solidification of Al dendrites but modifies the kinetics of the Al-Si eutectic [3]. Although the use of modifiers in Al-Si alloys promotes an improvement in mechanical properties, studies are still needed to clarify the influence of modifiers on the corrosion resistance. It is well known that structural parameters such as grain size and interdendritic spacing strongly affect corrosion resistance of as-cast alloys [4–6].

A. Garcia et al. investigated the effects of a eutectic modifier on the microstructure and surface corrosion behavior of Al-Si hypoeutectic alloys. In the study, modified and unmodified samples of an Al 9 wt % Si alloy were solidified under similar solidification conditions, and after metallographic procedures, the corrosion resistance was analyzed by both the electrochemical impedance spectroscopy technique and the Tafel extrapolation method carried out in a 0.5 M NaCl test solution at 25 °C. It was found that the Al 9 wt % Si alloy casting in the modified condition tends to have its corrosion resistance decrease when compared to the unmodified alloy. The study showed that hypoeutectic aluminum-silicon alloys could have significant improvements in mechanical properties by inducing structural modification in the normally occurring eutectic. The eutectic modification may affect not only the mechanical properties but also the corrosion resistance of such alloys [7].

Savaş has found that among casting parameters such as mold filling, liquid filtering, solidification time, and the dissolved hydrogen level of the liquid alloy and liquid treatments of molten alloy with the addition of Sr, the local solidification time and the dissolved hydrogen level of the melt were significant for microporosity formation [8]. Ruvalcaba found that streaming of solute-enriched liquid at the tip of high-order branches promotes growth by local undercooling. Further, solute advection and local solute rejection due to the local growth cause solute pile-up at the roots of the branches. This solute pile-up alters the local compositional balance at the solid–liquid interface at the root, causing the root to remelt, which in turn results in further branch detachment [9]. Boeira et al. [10] compared the experimental segregation profile and porosity evolution along the casting with theoretical predictions furnished by the numerical model, by considering a transient metal/mold heat transfer coefficient profile experimentally and determined that the numerical model depended on an experimentally determined heat transfer coefficient profile. A great agreement between the simulated profile and the experimental inverse copper profile was shown.

The simulation of porosity formation for an anisotropic channel has conformed better with the experimental scatter, with the experimental volumetric fraction of the pores profile presenting an ascending trend from the chill to the top of the ingot [10]. H. Combeau investigated the solidification of plates of different thicknesses in a sand mold. He calculated a maximum absolute pressure drop of 27,000 Pa in the 7.5-mm-thick casting whereas this maximum was only 300 Pa in the 30-mm-thick casting. Considering the condition of microporosity formation, these results showed the pressure drops were far too low to account for the formation of micropores that were observed experimentally. Hydrogen segregation had to be considered and integrated in a model to give a good prediction of micropore appearance [11]. E. Obaldia calculated the amount of hydrogen supersaturation based on the transport of dissolved hydrogen and Sieverts' law. An innovative aspect of his work was the extension of the model to make quantitative predictions of the volume fraction of porosity. Although the hydrogen supersaturation estimated the amount of porosity, these predictions were usually overestimated because the barrier of pore nucleation was not considered [12]. J. Li investigated electric current pulse (ECP) with parallel electrodes on the solidification structure of pure aluminum. The experimental results indicated that the solidification structure cannot be refined when the ECP is applied before the molten metal starts nucleating. However, significant refinement of the solidification structure could be achieved by applying ECP during the nucleation stage [13].

1.1.2 Grain Refiners

Understanding the crystallization process during solidification is an essential step to tailor the mechanical properties of solidified materials. The physical processes that govern crystallization are grain nucleation and the subsequent grain growth. In the industrial production process of aluminium alloys, the addition of titanium diboride (TiB₂) particles along with solute titanium is widely used to enhance the nucleation rate and control the grain growth during solidification. This procedure is generally referred as grain refinement. Although the mechanisms responsible for grain refinement have been extensively studied in

the last few decades, a comprehensive understanding is still lacking due to experimental difficulties in monitoring grain nucleation and growth in situ. The question of particular interest is how TiB_2 particles, along with solute titanium results in grain refinement, could be added, while no grain refinement is observed if one of the two is missing.

M. Zhang et al. have studied grain refinement in aluminum alloys using the edge-to-edge matching model. The researchers found excellent atomic matching between Al_3Ti nucleating substrates, known to be effective nucleation sites for primary Al, and the Al matrix in close-packed directions and close-packed planes containing these directions. The crystallographic features of the grain refiner and the Al matrix are consistent with the edge-to-edge matching model. For three other typical grain refiners for Al alloys, TiC (titanium carbide) (when $a=0.4328$ nm), TiB_2 , and AlB_2 , the matching occurs only between the close-packed directions in both phases and between the second close-packed plane of the Al matrix and the second close-packed plane of the refiners. According to the model, it is predicted that Al_3Ti is a more powerful nucleating substrate for the Al alloy than TiC , TiB_2 , and AlB_2 . This agrees with previous experimental results [14].

2. Modeling of Solidification Conditions and Melt Treatment in Microporosity Formation

2.1 Cooling Rate

The cooling rate plays an important role in determining the microstructure of casting. A higher cooling rate reduces the solidification time and grain size of the casting. Hence, grain density increases with the cooling rate. According to experimental observation, the average pore size decreases as the cooling rate increases. There are a number of explanations for this phenomenon. For a higher cooling rate, the dendrite arm spacing (DAS) decreases as do intergranular regions. Pore growth is thus limited. Another explanation is that with decreased solidification time, there is less time for hydrogen to diffuse from the solidifying dendrite to the liquid. Hence, the gas pore growth rate is inhibited.

2.2 Modifier

Eutectic modifiers are usually added to molten aluminium-silicon alloys to refine the eutectic phase particle shape and improve the mechanical properties of the final cast products. For aluminium-silicon alloys, this usually involves the addition of Sr or Na. In general, it is observed that modified castings contain more porosity than unmodified castings. Some possible reasons have been proposed and studied. In general, these reasons can be categorized as increasing inclusion content in the melt:

- decreasing hydrogen solubility in solid metal
- changing the solid/liquid interface morphology
- reducing the surface tension of the liquid metal
- increasing the volumetric shrinkage

2.3 Grain Refiner

The effects of grain refiners on porosity are still under study. In general, it has been observed that the addition of grain refiners increases the number of grain nucleation sites, thus reducing grain size. It has been shown that grain refinement reduces both the volume fraction of porosity and the pore size in A356 [15].

3. Model Formulation

In this section, the grain structure evolution model will be presented. The model of gas pore evolution is then described. Finally, the technique for coupling these two models is illustrated in detail.

3.1 Grain Structure Evolution Modeling

Grain nucleation and growth are two phenomena that influence microstructure evolution during the solidification of a casting. In this research, we will model heterogeneous nucleation and growth, a reasonable assumption for commercial casting.

3.1.1 Grain Nucleation

To model heterogeneous nucleation in solidifying casting, two methods have been proposed: an instantaneous model and a continuous model. The instantaneous model assumes all nuclei are formed at a given undercooling temperature. The continuous model assumes nucleation will occur continuously between the equilibrium temperature (i.e., as the liquid undercools) and the maximum undercooling temperature. Due to simplicity in program implementation, an instantaneous nucleation model is employed in the present study. Using this method, the grain density at a given location can be determined by correlation with the cooling rate, R :

$$N = k_1 + k_2 R + k_3 R^2, \quad (1)$$

where k_1 , k_2 , and k_3 are parameters that need to be determined by empirical analysis of the cooling rate and grain size in a real casting. Processing conditions, such as the addition of grain refiner, eutectic modifiers, and inclusion content, are known to influence the relationship between the grain density and the cooling rate.

3.2.1 Dendrite Growth and Orientation

There is a preferred crystallographic orientation for each grain. In our model, each equiaxed grain nucleated in the bulk of the casting is given a principal growth direction, a random positive integer with uniform distribution between 1 and 48. Each integer corresponds to a defined crystallographic orientation in two dimensions.

The dendrite growth kinetics can be calculated with the aid of the Kurz-Giovanola-Trivedi (KGT) model [26, 27]. The relationship between the dendrite tip velocity and the

undercooling temperature for the Al-7%Su alloy calculated by a KGT model is shown in Figure 3.

In our model, a two-dimensional (2-D) grid is generated from a given location in the casting where the microstructure and porosity prediction are of interest. The site of the grid scales directly from the computational elements used in macroscopic simulation. The element size of the grid in general is much finer than that of the control volume or element size used in a macroscopic heat transfer calculation. The three-dimensional (3-D) heat transfer calculation result, such as temperature and solid fraction, for each control volume is then mapped to a 2-D grid. The isothermal condition in every element is assumed, so the temperature profiles of an element are applied uniformly to its cells. It is assumed that the microstructure evolution does not influence the local thermal parameters. While such an assumption may not reflect the physical reality, it is a necessary assumption to apply a 2-D model to a 3-D process.

3.2 Gas Pore Evolution Modeling

The conditions for a gas pore to grow in the solidifying melt is that the gas pressure, P_g , has to be equal to or greater than the critical pressure, P_c :

$$P_g \geq P_c \quad (2)$$

The critical pressure is defined as

$$P_c = P_a + \rho_L gh + P_s + P_\sigma, \quad (3)$$

where P_a , $\rho_L gh$ and P_s are the ambient pressure, metallostatic pressure, and shrinkage pressure and surface tension per unit area P_σ between gas and liquid, respectively. P_a and $\rho_L gh$ are usually constants. P_g and P_s can be calculated as shown below. Assuming that the pore is circular and that the surface tension per unit area between gas and liquid is isotropic, P_σ is given by the well-known equation:

$$P_\sigma = \frac{2\sigma_{LG}}{r}, \quad (4)$$

where σ_{LG} is the surface tension between gas and liquid, and r is the radius of the pore [29].

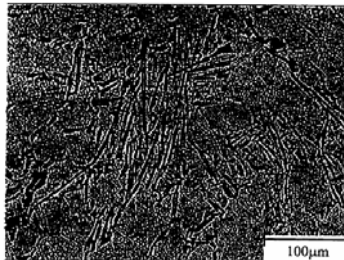


Figure 1: Typical microstructure of unmodified A356 alloy

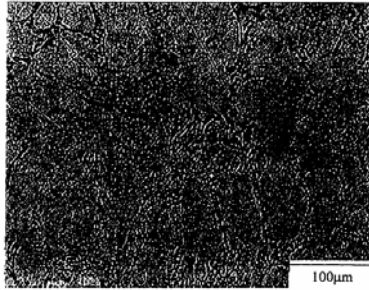


Figure 2 : Typical microstructure of Sr modified A356 alloy

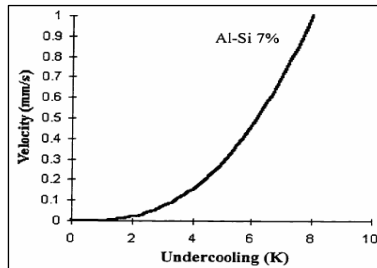


Figure 3: Dendrite tip velocity as a function of undercooling for A356 calculated by the KGT model

3.2.1 Computation of Gas Pressure

In most mathematical models for aluminium alloys, it is assumed that the hydrogen concentrations in liquid and solid at the solidification temperature are in equilibrium. To verify this assumption, the hydrogen diffusivity was calculated, and the dendrite arm spacing of the specimen was observed. The diffusivity of hydrogen, D (cm/sec), in solid aluminium is given as [19]:

$$D = 0.11 \exp\left(\frac{-110950}{RT}\right), \quad (5)$$

where R is the ideal gas constant ($\frac{J}{mol K}$). From equation 5, at $T = 823K$, $D = 1 \times 10^{-8} \frac{cm}{s}$.

The diffusion distance, λ , is defined as:

$$\lambda = \sqrt{2D\tau}, \quad (6)$$

where τ is the diffusion time. Given the diffusion time, the diffusion distance can be calculated from equations 5 and 6. For a permanent mold gravity casting, the solidification time is about 5–10 seconds. Therefore, the diffusion distance is about 5 μm .

The size of the dendrite arm for the A356 casting specimen used in this study (to be discussed) is shown in Figure 4. It can be seen that the size for half the dendrite arm is approximately 10 μm . Since the diffusion distance and size of dendrite arm are of the same

order, the hydrogen atoms can be assumed to have enough time to diffuse from solid to liquid in the permanent mold Al alloy casting used in this study.



Figure 4: Size of dendrite arms for A356 casting specimens

The complete equilibrium condition leads to:

$$\frac{[H_L]}{K_L} = \frac{[H_S]}{K_S}, \quad (7)$$

where $[H_L]$ and $[H_S]$ are the hydrogen concentrations in the liquid and solid metal, respectively, and K_L and K_S are constants described below.

Before the formation of the gas pore, the hydrogen mass balance equation is given as:

$$(1 - f_s)[H_L] + f_s[H_S] = [H_0], \quad (8)$$

where f_s is the solid fraction and $[H_0]$ is the initial hydrogen content in the melt. In addition, the mass concentration of hydrogen dissolved in solid and liquid metal is governed by Sieverts' law:

$$[H_S] = K_S P_g^{1/2} \text{ and } [H_L] = K_L P_g^{1/2}, \quad (9)$$

which yields equation 7 for equilibrium conditions.

Combining equations 8 and 9, the gas pressure before gas pore formation can be calculated as:

$$P_g = \left(\frac{1}{K_S^2}\right) \left(\frac{[H_0]^2}{\left[\left(\frac{K_L}{K_S}\right) - \left(\frac{K_L}{K_S} - 1\right)f_s\right]^2} \right) \quad (10)$$

The gas pressure increases as solidification proceeds. From equation 10, the maximum pressure can be computed as:

$$P_{g,\max} = \frac{[H_0]^2}{K_S^2} \quad (11)$$

Following classical nucleation theory, no gas pore will form if the maximum gas pressure, $P_{g,\max}$, is less than the critical pressure, P_c . Combining equations 3 and 11 allows us to

approximate the critical initial hydrogen content, $[H_0]_C$, above which a gas pore can form in the melt. From equation 3, $P_c \approx 2.75$ atm. If we assume $P_a = 1$ atm, then $h = 0.2$ m, $\sigma_{LG} = 0.79$ N/m [20], $r = 10 \mu\text{m}$, and the negative shrinkage pressure is neglected. Thus,

$$\frac{[H_0]_C^2}{K_s^2} = P_c, \quad (12)$$

that is,

$$[H_0]_C = K_s \sqrt{P_c}. \quad (13)$$

In this case, when $K_s = 0.062 \frac{\text{ml}}{100\text{g} * \text{atm}^{1/2}}$,

then $[H_0]_C = 0.10 \text{ml}/100\text{g}$. It should be noted that the critical initial hydrogen content depends on many factors such as alloy composition, solidification condition, etc. Therefore, the above approximation provides an indication of the relationship between the initial hydrogen content in the melt and the critical pressure.

When the initial hydrogen content is greater than the critical hydrogen content, gas pressure will form at the critical solid fraction during solidification. From equations 8 and 9, the critical solid fraction can be found as:

$$f_c = \frac{\frac{K_L - [H_0]}{K_s} - \sqrt{P_c}}{\left(\frac{K_L}{K_s} - 1\right)} \quad (14)$$

Note that f_c decreases as $[H_0]$ increases and P_c decreases. When the initial hydrogen content is high, the melt will reach the domain where gas pores will form at an earlier stage of solidification. Also, the addition of eutectic modifiers in the melt reduces the surface tension of the liquid aluminium alloy, which results in the reduction of P_c (equations 3 and 4). Hence, the critical solid fraction is reduced, and gas pores can nucleate earlier and grow over a longer period of time.

When the gas pore formation condition is satisfied as defined in equation 2, some hydrogen will be trapped in the gas pore. The hydrogen mass balance equation in this case is given as

$$[H_0] \rho_L = [H_s] \rho_s f_s + [H_L] \rho_L (1 - f_s - f_v) + \alpha \frac{f_v P_g}{T}, \quad (15)$$

where $[H_0]$ is the initial hydrogen content in the melt; $[H_s]$ and $[H_L]$ are the hydrogen contents in the solid and liquid; ρ_L and ρ_s are the densities for liquid and solid metal; f_s and f_v are the volume fraction of solid and porosity; α is a gas conversion factor; P_g is gas pressure; and T is the temperature. The last term in the equation represents the amount of hydrogen trapped in the gas pore. By substituting equation 9 into equation 15, the gas pressure after the gas pore has formed can be computed.

3.2.2 Computation of Shrinkage Pressure

The shrinkage pressure associated with liquid metal flow in the mushy zone represents the contribution of solidification shrinkage in microporosity formation. To determine the shrinkage pressure, the mass conservation equation must be solved:

$$\left(\frac{\rho_s}{\rho_L} - 1\right) \frac{\partial f_s}{\partial t} - \frac{\partial f_v}{\partial t} + \text{div}(f_L \bar{u}) = 0, \quad (16)$$

where ρ_s and ρ_L are densities of solid and liquid metal; f_s , f_v , and f_L are fractions of solid, porosity, and liquid; t is time; and \bar{u} is the interdendritic flow velocity vector. The first term in equation 16 represents the volume shrinkage associated with solidification. This shrinkage is compensated for by the growth of gas porosity or by liquid metal feeding. The interdendritic flow velocity, \bar{u} , can be calculated by Darcy's law [20]:

$$\bar{u} = -\frac{K}{\mu f_L} (\nabla P + \rho_L g t), \quad (17)$$

where K is the permeability of the medium, μ is the viscosity, f_L is the volume fraction of the liquid, P_s is the shrinkage pressure, ρ_L is the density of the liquid, g is the acceleration due to gravity, and t is the unit vector along the direction of gravity. The permeability is defined as:

$$K = \frac{f_L^3 d_2^2}{180(1 - f_L)^2}, \quad (18)$$

where d_2 is the secondary dendrite arm spacing. The pressure can be calculated by solving equations 16 through 18 simultaneously.

3.2.3 Pore Formation

Pore formation is a complex phenomenon. For the existing mathematical models, the initial nucleus size is usually assumed to be a fraction of the secondary dendrite arm spacing [20] or a very small number ($1 \mu m$). In our model, the pore nucleus radius is assumed to be equal to half the size of the cell ($5 \sim 10 \mu m$).

Equation 2 shows that the gas pore can form only when its pressure is sufficiently large to overcome the total local external pressure. After every term contributing to equations 2 and 3 is obtained by solving the basic equations, the program then checks and decides whether the pore formation condition is met, i.e., the gas pressure is greater or equal to the sum of the local liquid metal pressure and surface tension. If the condition is satisfied, a gas pore is formed and is stable. The program then randomly selects a liquid cell and assigns it to become a gas pore.

3.2.4 Pore Growth

As solidification continues, more hydrogen atoms are rejected from the growing solid into the liquid. If the pressure of the dissolved hydrogen is sufficient, the pore can grow.

During each time step, the pressure terms are calculated for every element in the location of interest. The calculation is reported until there are no liquid cells remaining in the elements, i.e., until solidification is complete.

3.3 Coupling of Grain Structure and Pore Evolution Models

In the micro-model, the time step used in the calculation should be determined first. From the KGT model, the dendrite tip velocity $V(\text{mm/s})$ is known given an undercooling temperature, (Figure 3). With a pre-defined cell size $d (\mu\text{m})$, the time step $\Delta t(\text{s})$ can be calculated:

$$\Delta t = \frac{d}{V} \quad (19)$$

After the time step has been determined, the microstructure prediction model starts with random selection of nucleation sites. The selections are made in every element in the two-dimensional grid when the element reaches the specified undercooling temperature. The number of nuclei that will form every element is calculated:

$$p = x \times \left(\frac{N}{n} \right), \quad (20)$$

where x is a random number that is uniformly distributed between 0 and 1, N is the number of liquid cells available in the element and n is the grain density of the element. A nucleus will form if $p \leq 1.0$. For every element, N is decreased by one after each iteration. On the other hand, the grain density of the element, n , is decreased by one only when the nucleus is formed (i.e., $p \leq 1.0$). A flow chart for this random cell selection process is shown in Figure 5.

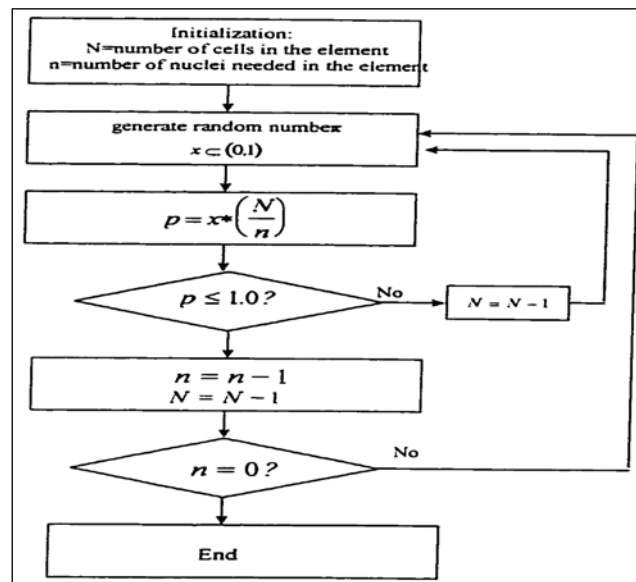


Figure 5: Flow chart for grain nucleus selection

In subsequent time steps, equiaxed grain growth is simulated. Since it is assumed that all the nuclei are formed at the same undercooling temperature, the dendrite tip growth velocity will be the same for all nuclei (Figure 3). With the number of nuclei in every element determined,

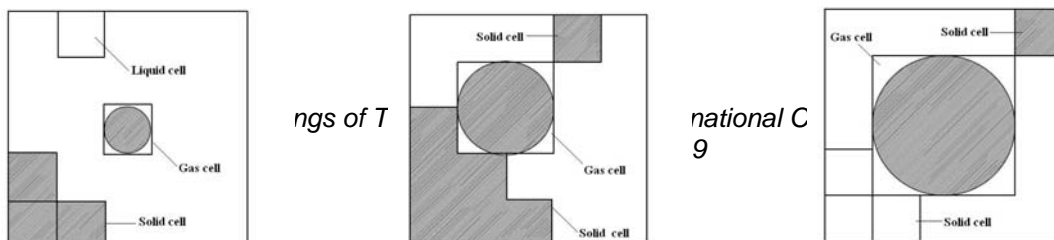
one could find the dendrite growth velocity that corresponds to the change in the solid fraction calculated by the macro-model. After the growth velocity is determined, one needs to choose the time step used in the micro-model calculation. In the micro-model, a solid cell grows with the square of the von Neumann nearest-neighbor configuration; however, it should be noted that the dendrite tip correction scheme is not incorporated in our model.

From experimental observations, it is known that hydrogen gas pores form in a spherical shape in the melt [8]. The difference in pore shapes depend on whether the pores are able to grow without obstruction or whether they are obstructed to a greater or lesser extent by other dendrites growing in the melt [8, 9]. In the simulation, when the gas pore growth condition is satisfied, growth occurs incrementally in steps determined by cell size.

Figure 6 is a schematic for the cellular automation used to simulate gas pore growth in the model. As mentioned before, the radius of the initial gas pore is assumed to be one-half the cell size; this means that the gas pore will occupy one cell in the element, as shown in Figure 6(a). During the next time step in the micro-model, if a gas pore has already formed, the program will check the possibility for growth. By assuming that the gas pore grows in increments of half the cell size, the gas pore will have a radius equal to one cell size. This means that the gas pore will occupy four cells in the element, as shown in Figure 6(b). As growth proceeds, the gas pore then has a radius equal to one and a half of the cell sizes. Thus, the gas pore will occupy nine cells in the element, as shown in Figure 6(c) and so on. In this way, gas pores can grow radially (for two dimensions) as observed in the experiment [8].

If gas pores cannot grow radially (i.e., near the end of solidification process when most of the molten metal has solidified), it is assumed that gas pores will expand to the remaining liquid cells that surround the pores, if any. With this assumption, the expansion of gas pores within a growing dendrite network can be simulated. During the solidification process, shrinkage pores will form because some of the liquid cells will be engulfed by solid, thereby choking the flow of the feeding liquid. In the model, the formation of isolated shrinkage pores is checked after every iteration (Figure 7).

With the algorithm described above, a gas pore will be able to grow circularly if it is formed at an early stage of solidification. During this time, the casting is mostly molten metal. It is not difficult for the gas pore to find the liquid pool that is needed for the pore to grow radially. As solidification progresses, the growth of the gas pore will be influenced by the advancing dendrite network. In the model, when a gas pore cannot grow radially, it will expand between the dendrites.



ngs of T

national C
9

(a) (b) (c)

Figure 6: Schematic for the cellular automation used to simulate gas pore growth

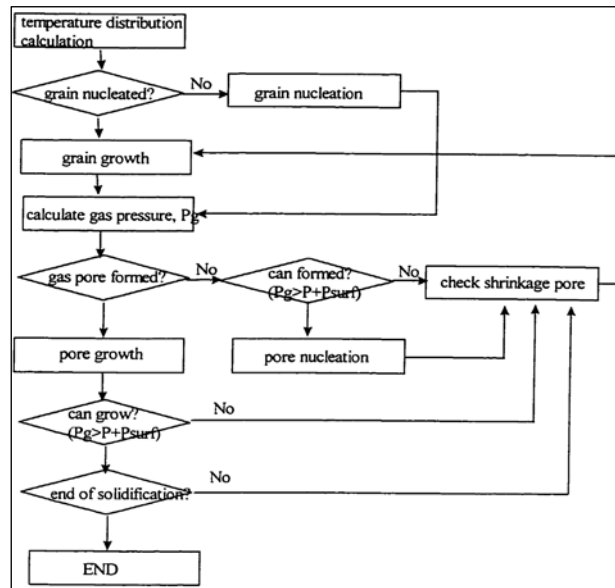


Figure 7: Flow chart of the proposed model

3.4 Shrinkage-induced Microporosity

Cast metal parts are sometimes unusable because they have large internal gas pockets, or porosity, that develops when the metal shrinks during solidification. Most large-scale porosity can be eliminated by a careful design of the casting mold to keep extra liquid metal in special regions for feeding the shrinkage. When metal can flow to compensate for shrinkage, porosity usually does not occur.

Another type of porosity is referred to as microporosity because it usually appears as a distribution of small bubbles whose total volume fraction is typically about 1 percent or less. Having a means of predicting the location and magnitude of microporosity is therefore of considerable interest. FLOW-3D's microporosity model has been developed for this purpose. The passive nature of the microporosity model means that it may be used in conjunction with macroporosity models and with either a pure heat conduction simulation or with full hydrodynamic simulations that include filling and solidification processes.

When a chill plate is inserted between the metal and the sand (on the top, bottom, and end surfaces), a spatially uniform metal temperature is no longer possible, and the solidification changes dramatically. There is zero microporosity near the chill plate where the cooling rate is largest, and the local temperature gradient in the metal is large. In this region, the metal reaches complete solidification before the adjacent metal reaches a critical solid fraction (and consequently is able to feed the shrinkage).

Figure 8 shows the computed microporosity along a centerline in the wedge together with the measured microporosity. Although the computed values are consistently lower, the general agreement is quite good. Both the measured and computed values are zero near the chill end, and both exhibit maximum values at the thick end of the wedge. These limits are what would be expected. The computed values plotted in Figure 8 are those along the wedge centerline and have not been area-averaged.

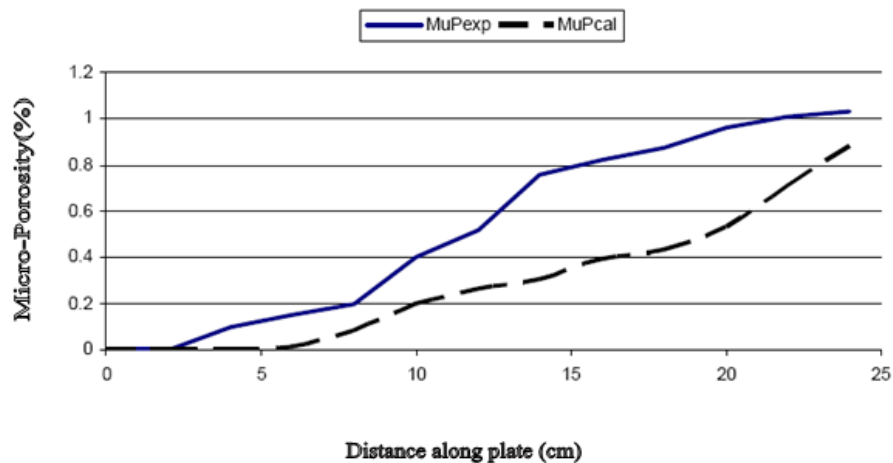


Figure 8: Microporosity measured (solid line) and computed (dashed line) in wedge

4. Conclusions

A two-dimensional model to predict pore size, morphology, and location has been developed for an A356 aluminium alloy solidifying under equiaxed grain structure conditions. To improve upon the conventional deterministic approach, the model links hydrogen gas evolution and microporosity formation mechanisms with a probabilistic grain structure evolution model with reasonable confidence. This information can then be used to evaluate the static and dynamic mechanical performances of casting during the earliest stage of product definition.

The following conclusions are drawn from this study:

1. For a permanent mold, Al alloy casting, the diffusion distance and size of the dendrite arm are of the same order. Hence, the approximation of complete equilibrium for hydrogen dissolved in solid and liquid can be assumed.
2. As solidification proceeds, no gas pore forms until the hydrogen gas pressure reaches a critical value.
3. There exists a critical initial hydrogen content below which the gas pore cannot form the melt. The critical initial hydrogen content depends on many factors such as alloy composition, solidification condition, etc.
4. When the initial hydrogen content is greater than the critical hydrogen content, gas pores will form at a critical solid fraction during solidification. The critical solid fraction decreases as the initial hydrogen content in the melt decreases and critical pressure decreases.
5. From experimental observation, the addition of grain refiner, 0.07 wt % TiB_2 decreases the grain size, pore area fraction, and pore size of the casting. In addition, it is observed that pores are more uniformly distributed.
6. In addition to grain refinement, the cooling rate has a strong influence on the grain size.
7. The model has been tested against three experimental data sets. Two tests involved a rectangular plate, and one involved a wedge. The model produces consistent approximations for all cases. It gives good qualitative distributions and reasonable quantitative results.
8. In some ways, the present microporosity model is similar to a temperature and temperature-gradient functional criteria method for estimating shrinkage induced microporosity.

References

- [1] S. M. Miresmaeili, J. Campbell, S. G. Shabestari, and S. M. A. Boutorabi, "Precipitation of Sr-rich Intermetallic Particles and Their Influence on Pore Formation in Sr-modified A356 Alloy," *Metallurgical and Materials Transactions A*, Vol. 36, no. 9, Sept. 2005, pp. xx–xx.
- [2] C. M. Dinnis, A. K. Dahle, J. A. Taylor, and M. O. Otte, "The Influence of Strontium on Porosity Formation in Al-Si Alloys," *Journal of Metallurgical and Materials Transactions A*, Vol. 35, no. 11, Nov. 2004.
- [3] E. Martínez, D. M. Cisneros, G. S. Valtierra, and J. Lacaze, "Effect of Strontium and Cooling Rate upon Eutectic Temperatures of A319 Aluminum Alloy," *Scripta Materialia*, Vol. 52, no. 6, 2005, pp. 439–443.
- [4] W. R. Osorio, C. M. A. Freire, A. Garcia, *Journal of Alloys and Compounds*, Vol. 397, , 2005, p. 179.

- [5] W. R. Osorio, J. E. Spinelli, N. Cheung, A. Garcia, *Materials Science and Engineering*, Vol. 420A, no. 179, 2006.
- [6] W. R. Osorio, C. M. A. Freire, and A. Garcia, *Journal of Material Science*, Vol. 40, 2005, p. 4493.
- [7] W. R. Osório, N. Cheung, J. E. Spinelli, P. R. Goulart, and A. Garcia, "The Effects of a Eutectic Modifier on Microstructure and Surface Corrosion Behavior of Al-Si Hypoeutectic Alloys," *Journal of Solid State Electrochemistry*, March 2007, pp. 1421–1427.
- [8] O. Savaş and R. Kayikci, "Application of Taguchi's Methods to Investigate Some Factors Affecting Microporosity Formation in A360 Aluminium Alloy Casting," *Materials & Design*, Vol. 28, 2007, pp. 2224–2228.
- [9] D. Ruvalcaba, R. H. Mathiesen, D. G. Eskin, L. Arnberg, and L. Katgerman, "In Situ Observations of Dendritic Fragmentation due to Local Solute-enrichment during Directional Solidification of an Aluminum Alloy," *Acta Materialia*, Vol. 55 2007, pp. 4287–4292.
- [10] A. P. Boeira, I. L. Ferreira, and A. Garcia, "Modeling of Macrosegregation and Microporosity Formation during Transient Directional Solidification of Aluminum Alloys," *Materials Science and Engineering A*, Vol. 435/436 2006, pp. 150–157.
- [11] H. Combeau, D. Carpentier, J. Lacaze, and G. Lesoult, "Modelling of Microporosity Formation in Aluminium Alloys Castings," *Materials Science and Engineering*, Vol. 173, pp. 155–159.
- [12] E. Obaldia and S. D. Felicelli, "Quantitative Prediction of Microporosity in Aluminum Alloys," *Journal of Materials Processing Technology*, Vol. 191, 2007, pp. 265–269.
- [13] J. Li, J. Ma, Y. Gao, and Q. Zhai, "Research on Solidification Structure Refinement of Pure Aluminum by Electric Current Pulse with Parallel Electrodes," *Materials Science and Engineering*, In Press, 2008.
- [14] M. Zhang, P. Kelly, M. Easton, and J. Taylor, "Crystallographic Study of Grain Refinement in Aluminum Alloys Using the Edge-to-edge Matching Model," *Acta Materialia*, Vol. 53, no. 5, 2005, pp. 1427–1438.
- [15] A. Knuutinen, K. Nogita, S. D. McDonald, and A. K. Dahle, "Porosity Formation in Aluminium Alloy A356 Modified with Ba, Ca, Y and Yb," *Journal of Light Metals*, 2001, pp. 241–249.
- [16] W. Kurz, B. Giovanola, and R. Trivedi, "Theory of Microstructural Development During Rapid Solidification," *Acta Metallurgica*, Vol. 34, 1986, pp. 823–830.
- [17] J. L. Spittle and S. G. R. Brown, "Computer Simulation of the Effect of Alloy Variables on the Grain Structures of Castings," *Acta Metallurgica*, Vol. 37, 1989, pp. 1803–1810.
- [18] M. E. Fine, *Introduction to Phase Transformations in Condensed Systems*, Macmillan Co., 1964, p. 7.
- [19] E. A. Brandes and G. B. Brooks (editors), *Smithells Metals Reference Book 7th ed.*, Butterworth-Heinemann, 1992, pp. 13–72.
- [20] J. D. Zhu and I. Ohnaka, "Computer Simulation of Interdendritic Porosity in Aluminum Alloy Ingots and Casting," *Modeling of Casting, Welding and Solidifications Processes*, 1991, pp. 435–442.